Journal of Catalysis 271 (2010) 161–169

Contents lists available at ScienceDirect

Journal of Catalysis

journal homepage: www.elsevier.com/locate/jcat

Control of the thickness of mesoporous titania films for application in multiphase catalytic microreactors

Lidia N. Protasova [a,b], Evgeny V. Rebrov [a], Tatiana S. Glazneva [b], Angel Berenguer-Murcia [c], Zinfer R. Ismagilov [b], Jaap C. Schouten [a,*]

[a] Eindhoven University of Technology, P.O. Box 513, 5600 MB Eindhoven, The Netherlands
[b] Boreskov Institute of Catalysis, Pr. Lavrentieva, 5, Novosibirsk 630090, Russia
[c] Departamento de Química Inorgánica, University of Alicante, Ap. 99 – 03080 Alicante, Spain

ARTICLE INFO

Article history:
Received 14 May 2009
Revised 23 July 2009
Accepted 27 July 2009
Available online 7 March 2010

Keywords:
Mesoporous titania films
Au nanoparticles
Citral hydrogenation

ABSTRACT

A new method of sol–gel polymer template synthesis of mesoporous catalytic thin films has been proposed which allows controlling the chemical nature of the film, the porosity, thickness and loading with an active species. The mesoporous films with a long-order structure can be obtained in a narrow range of surfactant-to-metal precursor molar ratios from 0.006 to 0.009. The catalytic film thickness was varied from 300 to 1000 nm while providing a uniform catalyst distribution with a desired catalyst loading (1 wt. % Au nanoparticles) throughout the film. The films were characterized by TEM, SEM, ethanol adsorption and contact angle measurements. The calcination of the as-synthesized films at 573 K reduced Ti^{4+} sites to Ti^{3+}. A 300 nm thick Au-containing film showed an initial TOF of 1.4 s^{-1} and a selectivity towards unsaturated alcohols as high as 90% in the hydrogenation of citral. Thicker films demonstrated a high selectivity towards the saturated aldehyde (above 55%) and a lower intrinsic catalytic activity (initial TOF of 0.7–0.9 s^{-1}) in the absence of internal diffusion limitations.

1. Introduction

Catalytic microstructured reactors are becoming widely recognized for their unique properties and potential applications in chemical industry [1,2]. Their efficient use requires shaping of the catalyst usually by deposition of catalytic thin films on microchannel walls. Catalytic thin films can be produced on a substrate by different methods such as hydrothermal synthesis [3–7], anodic oxidation [8,9] and evaporation-induced self-assembly (EISA) [10,11]. The latter is a variant of sol–gel synthesis [12–14], where either spin-coating or dip-coating is applied for destabilization of the initial sol. This method enables the formation of highly ordered mesoporous films with various porous hierarchies.

Recently, mesoporous titania thin films have attracted considerable attention in catalysis due to their large surface areas, narrow pore size distribution and favourable surface properties [11,15,16]. The films obtained by either spin-coating or dip-coating have a narrow pore size distribution in the mesopore range but their thickness is limited to 300 nm, which prevents their efficient use in microstructured reactors as the catalyst occupies less than 0.5% of the reactor volume. There are several options to increase the film thickness, such as lowering the rotation speed during spin-coating (or increasing the solvent withdrawal speed during dip-coating) or increasing the viscosity of the initial sol. However, there is a narrow range of conditions leading to the formation of mesoporous structures rather than disordered macroporous films. For the synthesis of sol–gel derived mesoporous titania thin films, the precursors need to be partially hydrolyzed under controlled conditions, so that subsequent polycondensation reactions yield a weakly branched polymeric metal oxide sol [15,17–22]. The rates of hydrolysis and polycondensation reactions are controlled by the surfactant-to-metal precursor ratio, temperature, solution dilution level and pH [15].

The thickness of the mesoporous films can be increased by repeating the spin-coating, aging and calcination steps. Recently the layer-by-layer deposition method of Ag doped silica and titania films has been reported [23]. It is well known that the specific surface area and the mesopore volume can be markedly reduced during calcination, which may also lead to shrinkage of the internal layers in a multilayer film if the surfactant is not completely removed [21]. Therefore it is important to develop a calcination protocol which allows removal of the surfactant at the lowest possible temperature.

In order to assess the feasibility of the proposed deposition method, the catalytic performance of the single and multilayer

* Corresponding author. Fax: +31 40 244 6653.
E-mail address: j.c.schouten@tue.nl (Jaap C. Schouten).

0021-9517/$ - see front matter © 2009 Elsevier Inc. All rights reserved.
doi:10.1016/j.jcat.2009.07.013

coatings should be compared in a catalytic reaction. This has to be fast enough for application in microstructured reactors and should include several subsequent steps to evaluate the performance in terms of both activity and selectivity. Citral hydrogenation has been chosen as a test reaction as this is a multi-step reaction and the presence of internal diffusion limitations substantially decreases the selectivity towards the semihydrogenated products. Gold nanoparticles have been chosen as an active metal to test the performance of structured Au/TiO_2 catalysts in the hydrogenation of citral.

Classical ways of deposition of Au nanoparticles, such as impregnation and deposition–precipitation could provide a uniform distribution with the active metal with a high metal dispersion. Nevertheless, the low reproducibility of these methods severely limits their applicability when applied to manufacturing of structured catalysts. Furthermore, obtaining the desired loading with an active component in a single step is not straightforward [24]. On the other hand, the direct addition of metal nanoparticles into the Ti sol with subsequent aging and evaporation-induced self-assembly provides a good alternative to the post synthesis loading of the active component. The initial size and the chemical composition of the metal nanoparticles can be well controlled in a reduction by solvent method [24].

In view of the tailoring that is possible with microreactors, it is increasingly being recognized that major improvements in the selectivity of reactions can be achieved by changes in the catalyst and/or support structure rather than in process conditions. In this work a method is proposed to increase the thickness of catalytic mesoporous films while maintaining their morphology, long-range order and mesoporous structure. The particle size in a nanostructured catalyst, the pore size and the thickness of the mesoporous support can be independently controlled via a one-pot EISA synthesis. Prior to multi-step synthesis, the surfactant-to-metal precursor ratio should be optimized to obtain stable films with a long-order structure.

Calcination conditions suitable for complete surfactant removal have been investigated by FTIR to obtain crack-free films of known thickness which required complete stabilization of the inorganic framework before the next deposition cycle. The morphology of the films was studied by LA-XRD, TEM and ethanol adsorption–desorption isotherms. The film thickness was determined by ellipsometry and SEM. The strength of the different acid sites was studied by FTIR spectroscopy of adsorbed CO at 77 K. The activity of the resulting Au/TiO_2 catalysts was studied in the hydrogenation of citral.

2. Experimental

2.1. Preparation of mesoporous titania films

Silicon and titanium substrates with a cross-section of $9.8 \times 9.8\ mm^2$ and a thickness of 0.5 mm were used. Prior to film deposition, the surface roughness of the silicon and glass substrates was increased to 500 nm as described elsewhere [13]. Solution A was prepared by mixing titanium isopropoxide (99.99 wt.%, Fluka) and an aqueous HNO_3 solution (65 wt.%, Fluka) under vigorous stirring. Solution B was prepared by dissolving Pluronic F127 (EO_{100}–PO_{65}–EO_{100}, BASF) in ethanol (99.99 wt.%, Aldrich). After stirring for 1 h, solution B was added to solution A. The resulting solution with a molar composition of 1 $Ti(O–iC_3H_7)_4$: 0.005–0.009 Pluronic F127: 40 Ethanol: 1.3 H_2O: 0.13 HNO_3 was stirred for either 8, 15, 25 or 240 hours at 298 K (Fig. 1). After an aging period of 25 h, the solution was deposited on the substrates. The films were produced by spin-coating at 1500 rpm at a relative humidity (RH) of 80%. The as-deposited films were kept at a RH of 80% for 48 h and then were calcined at 573 K for 4 h under a residual pressure of 10 mbar with a heating rate of 1 K min^{-1}.

2.2. Preparation of Au/TiO_2 catalytic mesoporous films

A PVP-stabilized Au colloid solution in ethanol was prepared as shown in Fig. 2 and described elsewhere in detail [25,26].

Poly-*n*-vinyl pyrrolidone (1.14 g) was added to anhydrous ethylene glycol to make solution 1. For solution 2, 0.39 g of $HAuCl_4$ was dissolved in water. Then solution 2 was poured into solution 1 under stirring. The pH of the resulting mixture was adjusted to 9–10 by adding a NaOH solution. The resulting solution was heated at 373 K for 2 h after which it was cooled to room temperature. The prepared nanoparticles were purified as follows: an aliquot containing the desired amount of nanoparticles was treated with a large excess of acetone. This treatment produced the extraction of the protecting polymer to the acetone phase, provoking flocculation of the metallic nanoparticles. After removal of the acetone phase, the purified colloids were redispersed in ethanol [26]. The average size of the Au nanoparticles was obtained by taking several TEM pictures and measuring 100 individual nanoparticles in the colloid solution was found to be 4 nm [24].

A certain amount of the Au colloidal solution, calculated to obtain a 1 wt.% Au loading in the resulting mesoporous film, was mixed with Pluronic F127 at 323 K. Solution A (see Section 2.1) was added and the resulting mixture (solution C) was aged for

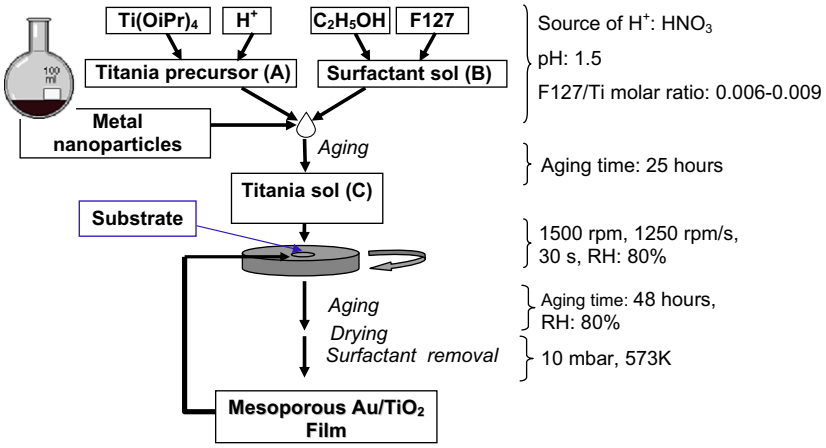

Fig. 1. Sol–gel synthesis of Au/TiO_2 multilayer catalytic coatings.

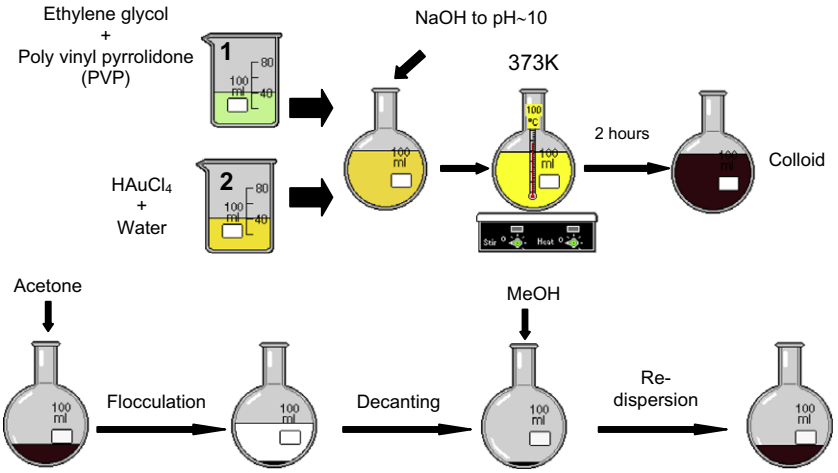

Fig. 2. A schematic view of the reduction by solvent method for the synthesis of Au nanoparticles.

2 h. The precursor/surfactant ratio was chosen to be 0.009, and the pH value was 1.5. The films were deposited on the titanium substrates as described in Section 2.1. Thicker films were prepared from solution C by consecutive repetition of spin-coating, aging and calcinations steps after every deposition (see Fig. 1).

All films are referred to as TiO_2(or Au/TiO_2)-*i*-*a*. The roman numerals (I, II or V) in the first index (*i*) denote the number of deposition cycles. The second index (*a*) stands for the surfactant-to-precursor molar ratio multiplied by 10^3. For example, a catalytic mesoporous film after 2 deposition cycles performed with a surfactant to precursor ratio of 0.009 will be referred as Au/TiO_2-II-9 hereafter.

2.3. Characterization

Low-angle XRD spectra were recorded on a Rigaku Geigerflex device with Cu K_α radiation (40 kV, 40 mA), 0.01–0.02° 2 theta step size, with a counting time of 4.0 s. 2D SAXS was performed with a rotating anode X-ray generator (copper anode operated at 50 kV, 30 mA; small focus) equipped with two adjustable optical systems. The Scanning Electron Micrographs (SEMs) were obtained on a Quanta 3D FEG microscope at 30 kV with a resolution of 1.2 nm. The Transmission Electron Micrographs (TEMs) were obtained on a JEM-2010 microscope at 200 kV with a resolution of 0.14 nm. Samples for TEM were prepared by placing a slice of the film removed from the substrate on a copper grid coated with a carbon film and dried under vacuum.

Surfactant removal was studied by FTIR on a BOMEM MB 102 spectrometer in the 200–4000 cm^{-1} range with a resolution of 4 cm^{-1}. CO adsorption at 77 K and 0.13 and 13 mbar was studied on a Shimadzu FTIR-8300 spectrometer in the region of 400–6000 cm^{-1} with a resolution of 4 cm^{-1} and accumulation of 100 scans. All FTIR studies were performed in a transmission mode on supported films without any destruction of the samples. Each experiment required one sample. Prior to CO adsorption, the sample was pretreated in an IR cell at 673 K for 2 h under a residual pressure of 0.01 mbar to remove adsorbed surface species. The strength of the Brønsted acidic sites is referred to as proton affinity (PA) determined from IR-spectra by Eq. (1):

$$PA_{OH} = PA_0 - \frac{1}{0.00226}\log(\Delta\upsilon_{OH}/\Delta\upsilon_{SiOH}), \quad (1)$$

where a PA_0 of 1390 kJ mol^{-1} is the proton affinity of aerosil hydroxyl groups which is used as standard, a $\Delta\upsilon_{SiOH}$ of 90 cm^{-1} is the frequency shift of the Si–OH vibration, and $\Delta\upsilon_{OH}$ is the frequency shift of the OH vibration. The $\Delta\upsilon_{OH}$ values were obtained from the FTIR differential spectra. The latter were obtained by subtraction of the spectrum of the pretreated sample from the spectrum taken at the maximum saturation value [27].

The mesopore volume of the films and pore size distribution were determined by Ellipsometric Porosimetry (EP) from the desorption branch of the ethanol isotherms at 287 K using the Bruggerman effective media approximation and the improved Deriaguin–Broekhoff–de Boer model. The film porosity was calculated with an accuracy of ±3% based on the change of the effective refractive index between the empty film and the film filled with ethanol [28]. The thickness of the mesoporous films was determined on an M-2000F EC-400 Spectroscopic Ellipsometer (J.A. Woollam Co., Inc.). The applied optical model consisted of three layers: a silicon substrate layer, a native silicon oxide layer of 3 nm and the mesoporous titania layer [28]. The contact angle of a water droplet of 2 μl on the substrates was measured on a Dataphysics OCA 30 device at 293 K and a RH of 40%.

2.4. Catalytic activity

Fifty Au/TiO_2 films were clamped between two concentric rings at a distance of 1 mm from each other. These two rings were connected to a central shaft which was used for stirring. This holder was placed in an autoclave reactor with a total volume of 270 ml. Prior to activity measurements, the catalytic films were reduced *in situ* at 523 K at a H_2 pressure of 12 bar for 12 h to remove the surface oxygen. Then, the reactor was cooled to room temperature. The hydrogenation reaction was performed with 130 ml of a 0.01 M deoxygenated solution of citral in 2-propanol at 343 K and 12 bar H_2 pressure. The stirring speed of the holder equipped with the plates was 1500 rpm. Analysis of the reaction mixture was performed off-line with a Varian CP-3800 gas chromatograph equipped with a CP-Sil 5 CB capillary column (diameter: 1 mm, length: 30 m) and a FID detector. The carbon balance was closed within 99%. The turnover frequency (TOF) was calculated as follows: $TOF = X \cdot n_{C10H16O}/(t \cdot \alpha \cdot D \cdot n_{TiO2})$, where X is the citral conversion, $n_{C10H16O}$ is the initial amount of citral in the reactor, n_{TiO2} is the amount of the titania support in the reactor, α and D are the Au loading and dispersion, respectively, and t is the reaction time. The Au dispersion was estimated as $D \approx 0.9/d_{TEM}$ [29], where d_{TEM} is the average particle size as recorded using TEM (nm).

3. Results and discussion

3.1. Single layer mesoporous titania films

3.1.1. Influence of calcination temperature on the surfactant removal and film thickness

To identify the range of conditions under which stable mesoporous titania films with a long-order structure can be obtained, a series of single layer films were studied by several physical methods immediately after the synthesis as well as after storage in air for 2 months.

Surfactant removal and dehydroxylation during calcination were studied over the sample TiO_2-I-6 by FTIR. The most intense absorption bands of Pluronic F127 were observed in the FTIR spectra of the as-synthesized film at 1110 cm^{-1} and in the 2850–2930 cm^{-1} range (Fig. 3a). These bands were assigned to the C–O–C stretching, CH_2 bending and C–H stretching vibrations (see Table 1). They were used to monitor the surfactant removal during calcination. The formation of the Ti–O–Ti bridges during dehydroxylation of the terminal hydroxyl groups in the amorphous titania walls can be seen after calcination at 473 K (Fig. 3b). The complete removal of surfactant was achieved after calcination at 573 K for 4 h (Fig. 3c). It should be mentioned that film thickness decreases from 350 to 177 nm after calcination at 573 K due to a contraction of the titania framework in the direction perpendicular to the substrate. Therefore it is of importance to obtain complete surfactant removal and stabilization of the inorganic network before deposition of the next layer.

3.1.2. Influence of surfactant content in the sol on film porosity and stability

Fig. 4a–c shows the XRD patterns of the as-synthesized titania films TiO_2-I-6, TiO_2-I-7, (c) TiO_2-I-9, while Fig. 4d–f shows patterns of the same films after storage in air for 2 months (spent films). The average film thickness after calcination was 175 ± 5 nm. The unit cell parameter was calculated from the position of the (200) peak of a P6 mm hexagonal structure. The unit cell decreases from 10.8 nm in TiO_2-I-6 to 8.1 nm in TiO_2-I-9. No long-order structure was observed at a surfactant-to-precursor molar ratios below 6×10^{-3} and above 9×10^{-3} (not shown). All films have a 2D hexagonal structure (see 2D SAXS image in Fig. 4, frame). The pattern consists of well-defined diffraction spots [30], which are distributed along an ellipse rather than a circle. This confirms an anisotropic contraction of the films during calcination [15].

A long-order hexagonal structure was preserved in spent (after storage in air for 2 months) TiO_2-I-9 (Fig. 4f), while at a lower surfactant content (TiO_2-I-*a*, *a* = 6 and 7) it disappeared in the spent films (Fig. 4d and e). The XRD results were confirmed by the TEM image analysis of spent TiO_2-I-9 and TiO_2-I-7 (Fig. 5a and b, respectively). A highly ordered mesoporous domain was observed in the TEM of TiO_2-I-9. The average size of a unit cell, which includes one pore and one pore wall, is 9.0 nm (22 unit cells over 200 nm). This value is close to that obtained from the XRD results.

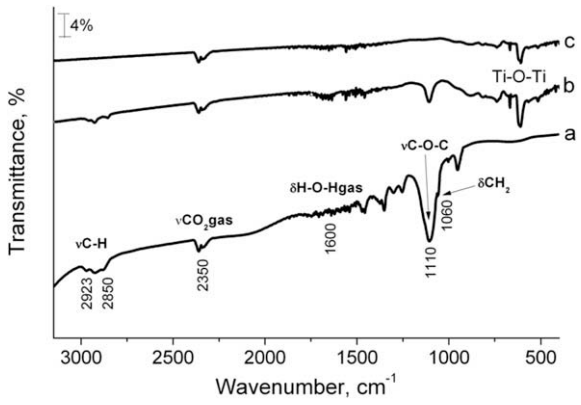

Fig. 3. FTIR spectra of (a) Pluronic F127 surfactant, and TiO_2-I-6 film calcined at (b) 473 K, (c) at 573 K.

Table 1
Vibration frequencies of different groups.

Vibration	Frequency (cm^{-1})	Reference
C–O–C stretching	1110	[46]
CH_2 rocking	1060	[47]
C–H stretching	2850 and 2923	[48]
CO_2 in gas phase stretching	2350	[49]
H–O–H bending	1600	[50]
Ti–O–Ti	430–860	[51]

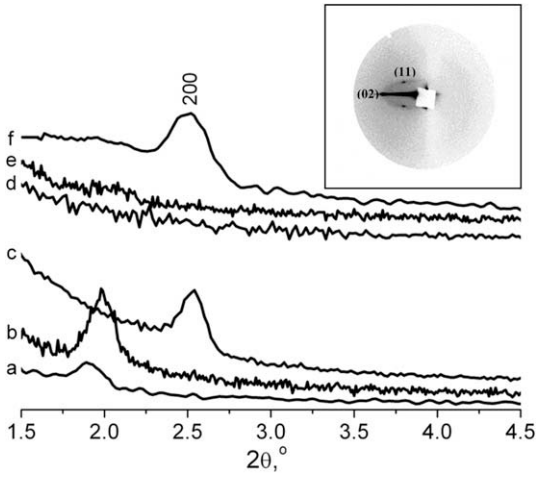

Fig. 4. LA-XRD patterns of mesoporous titania films: (a) TiO_2-I-6, (b) TiO_2-I-7, (c) TiO_2-I-9 as-synthesized, (d) TiO_2-I-6, (e) TiO_2-I-7, and (f) TiO_2-I-9 after storage in air for 2 months. A 2D SAXS image of TiO_2-I-9 is shown in the frame.

Typical adsorption–desorption isotherms of ethanol are shown in Fig. 6. Type IV adsorption isotherm with a hysteresis loop and a narrow PSD was observed, indicating a strong support–adsorbate interaction [31]. The mean pore size increased from 2.5 nm at *a* = 5 to 3.2 nm at *a* = 7 and finally to 3.5 nm at *a* = 9. These values are still lower as compared to 5 nm reported elsewhere [15]. The pore size distribution is narrow with a deviation of ±0.5 nm from the average value. Comparing the XRD, TEM and EP results it can be concluded that the thickness of the pore wall decreases with increasing surfactant content in the sol. The thickness of the pore wall can be calculated by subtracting the unit cell size from the pore size. As the unit cell size decreases, the pore wall thickness also decreases from 8.0 nm in TiO_2-I-6 to 4.5 nm in TiO_2-I-9. At the same time, the film porosity increases from 14% to 25% (Fig. 7). These data yield evidence that increasing the surfactant content increases the mean pore size and the mesopore volume due to a larger micelle size at higher surfactant concentrations in the sol [11].

Thus, a stable hexagonal mesoporous structure was obtained only at a F127/Ti molar ratio of 0.009. This ratio was used for the synthesis of supported titania catalysts with embedded nanoparticles.

3.1.3. Investigation of Lewis and Brønsted acidity by FTIR of adsorbed CO

Both Lewis and Brønsted acidities of the titania surface were determined by CO adsorption. The effect of different surfactant

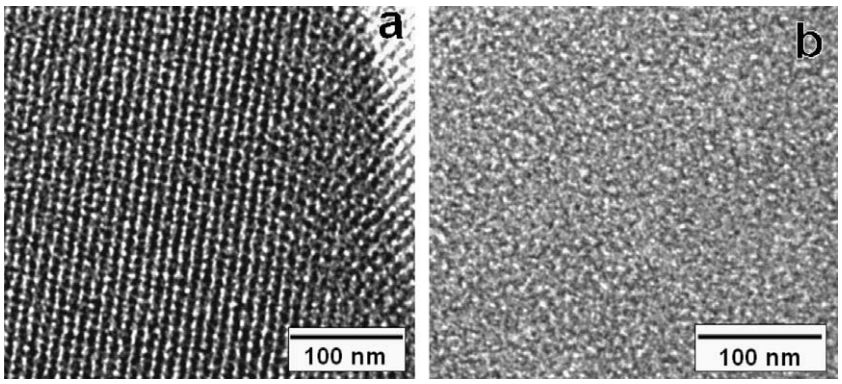

Fig. 5. TEM images of the mesoporous titania films taken after storage in air for 2 months: (a) TiO_2-I-9, and (b) TiO_2-I-7.

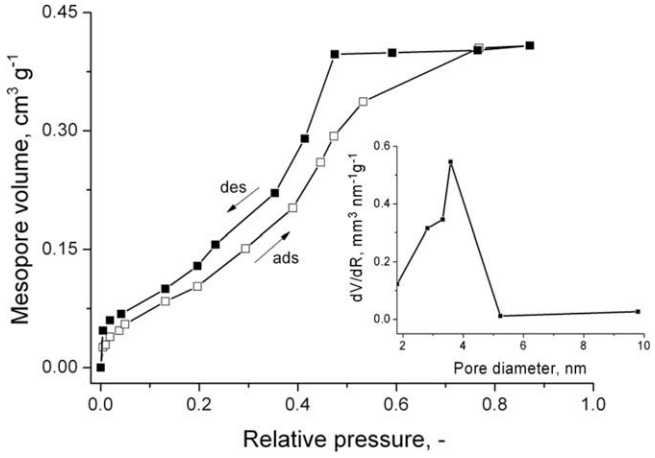

Fig. 6. Ethanol adsorption–desorption isotherms at 287 K and the pore size distribution for the film TiO_2-I-9.

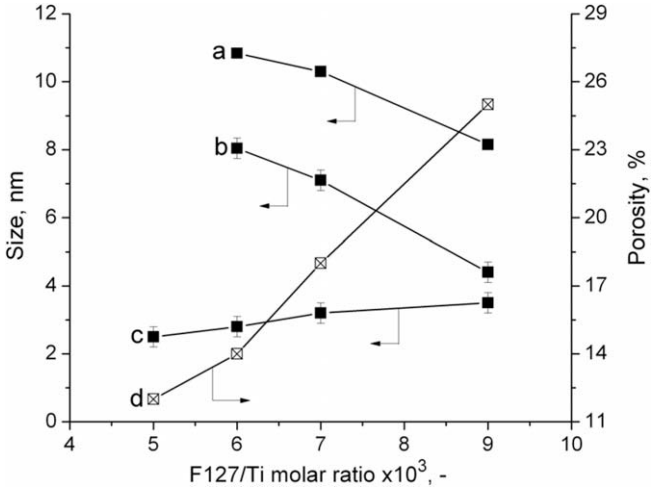

Fig. 7. Dependence of the porosity, pore and unit cell sizes, pore wall thickness of mesoporous titania films on surfactant-to-precursor molar ratio: (a) unit cell size, (b) pore wall thickness, (c) pore size, and (d) porosity.

content was studied over TiO_2-I-5 and TiO_2-I-9 by FTIR of adsorbed CO (Fig. 8). The adsorption bands at 2153 and 2156 cm^{-1} are assigned to CO adsorbed on the Ti–OH groups. The bands at 2141 and 2145 cm^{-1} are related to CO condensed in the mesopores (CO in gas phase) [27], while those at 2123 and 2129 cm^{-1} are

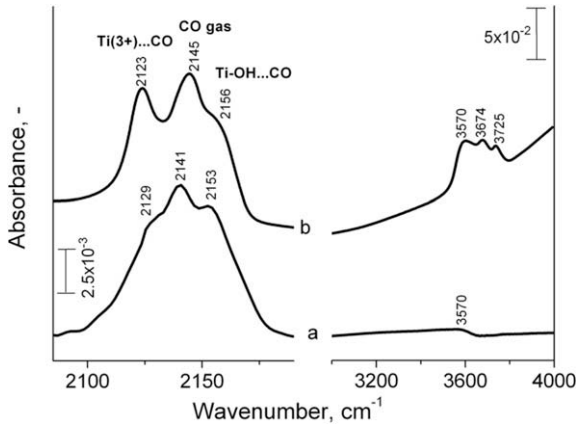

Fig. 8. FTIR spectra of CO adsorbed on: (a) TiO_2-I-9, (b) TiO_2-I-5. Experimental conditions: temperature 77 K, CO pressure 13 mbar. The sample was pretreated in an IR cell at 673 K for 2 h under a residual pressure of 0.01 mbar to remove adsorbed surface species.

characteristic for CO adsorbed on the Ti^{3+} species [32]. In both cases no adsorption band at 2180 cm^{-1} was observed, demonstrating the absence of unsaturated Ti^{4+} sites on the surface [33]. The reduction of the Ti^{4+} sites at 773 K gives the Ti^{3+} sites [34–37]. This effect was observed already at 573 K in [37]. However, further heating to 773 K significantly increased the amount of the reduced

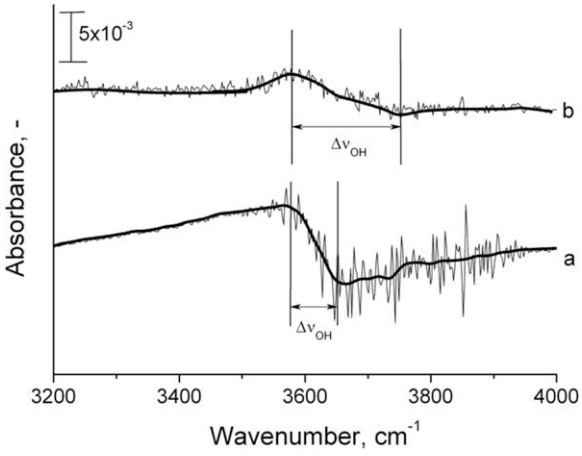

Fig. 9. Differential FTIR spectra of mesoporous titania films: (a) TiO_2-I-9, (b) TiO_2-I-5. Experimental conditions are the same as those in Fig. 8.

Table 2
Acidic properties of titania films determined by IR of adsorbed CO.

Sample	υ_{1CO} (cm^{-1})	υ_{2CO} (cm^{-1})	υ_{OH} (cm^{-1})	$\Delta\upsilon_{OH}$ (cm^{-1})	PA[a] (kJ mol)
TiO_2-I-5	2123	2156	3570, 3674, 3725	168	1270
TiO_2-I-9	2129	2153	3570	98	1373

[a] PA – proton affinity.

sites. In this study, the Ti^{3+} sites were formed after calcination of the mesoporous films at 573 K.

The frequency shift of the OH vibration ($\Delta\upsilon_{OH}$) was obtained from the FTIR differential spectra (Fig. 9, Table 2). The hydroxyl groups in both the films possess strong acidic properties.

Thus, pretreatment at 573 K at low pressure creates reduced Ti^{3+} sites in the mesoporous films.

3.1.4. Influence of porosity on hydrophilic properties

Surface hydrophilicity of films is an important parameter when they are applied in multiphase catalysis. In order to improve the interactions between a heterogeneous catalyst and the reactants flowing in the liquid film, it is of prime importance to ensure good wetting of the surface. High surface hydrophilicity provides stabilization of the liquid flow around the catalyst, which can substantially reduce the pressure drop in the microreactor. The surface concentration of hydroxyl groups was studied before and after UV-treatment by measuring the contact angle of a water droplet on the films obtained with different surfactant-to-precursor ratios (series TiO_2-I-*a*, where *a* = 5, 6 and 7). The initial contact angle was 35, 32 and 30 ± 1° over TiO_2-I-5, TiO_2-I-6 and TiO_2-I-7, respectively. After a UV-treatment for 2 h, the water contact angle decreased to 14 ± 1° over TiO_2-I-5. Samples TiO_2-I-6 and TiO_2-I-7 were more hydrophilic with contact angles of 9 ± 1° and 8 ± 1°, respectively. The film surface became superhydrophilic on all samples after 5 h of UV irradiation. In this state, the highest concentration of surface hydroxyl groups (>15 OH per nm^2) was created on the surface [22]. The difference of hydrophilicizing rate of films is related to their different mesoporosities. The films with a higher mesopore volume and larger surface areas enhance their hydrophilicity owing to the so-called two-dimensional capillary phenomenon [38,39].

Based on the results described above, it can be concluded that there exists a narrow range of the surfactant-to-metal precursor ratios between 0.006 and 0.009 leading to formation of mesoporous titania films with a high degree of long-order structure. The thickness of the pore wall decreases while the porosity and the long-term stability increase with increasing the surfactant content in the initial sol. A higher porosity is beneficial to rapid diffusion of the reactants and products, especially in thicker films. The templating agent can be completely removed from the film by calcination at 573 K at a residual pressure of 10 mbar for 4 h. Under these conditions Ti^{4+} sites are reduced to Ti^{3+}. A F127/Ti molar ratio of 0.009 and optimized calcination conditions were chosen for the synthesis of multilayer films.

3.2. Multilayer mesoporous catalytic titania films

After optimization of synthesis parameters for a single layer, Au-containing catalytic films with two, three and five consequent layers were synthesized and analyzed as described in Section 2.2 (Table 3). The thickness gain was almost the same in the first and second deposition cycles. The similarity of the deposition process indicates that the UV-induced superhydrophilic state of the surface has a minor influence on the thickness of the film layer. However, in the third and fifth deposition runs less material was deposited per deposition cycle. This might be related to an increased surface roughness of the films after multiple depositions. On the surface of spin-coated films derived from alkoxide solutions is often observed the so-called "radiative striation", i.e. circumferential unevenness in thickness or radially extended ridges. Striations can scatter the solution from the next deposition cycle resulting in a smaller growth rate. It can be seen from a cross-sectional view of the film in Fig. 10 that a significantly heterogeneous thickness profile is obtained after five deposition cycles. The mean film thickness is 1 μm; however, the film contains thicker and thinner areas with an on-scale difference of several tens of micrometres. In spite of non-uniform growth rate, a proportional weight gain confirms uniform porosity throughout the film.

Table 3
Characteristics of mesoporous films Au/TiO_2-*i*-9.

Number of deposition cycles	Thickness (nm)	Weight[a] (mg)	Apparent density[b] (g cm^{-3})	Initial TOF (s^{-1})
1	300	0.6	0.40	1.4
2	590	1.1	0.37	0.7
3	660	1.3	0.39	n.d.
5	1000	2.0	0.40	0.9[c]

n.d. – not determined.
[a] Weight is given for fifty films on substrates of 9.8 × 9.8 mm^2.
[b] Apparent density is given as weight divided by the coating volume.
[c] TOF decreased to 0.26 s^{-1} in 16 min.

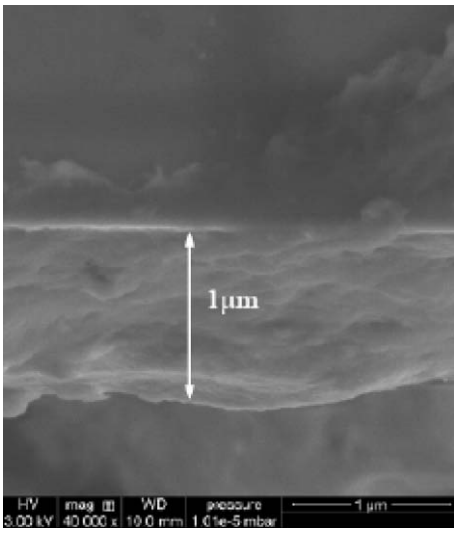

Fig. 10. SEM image of Au/TiO_2-V-9.

A narrow pore size distribution with a mean pore size of 3.1 ± 0.2 nm was observed on the Au/TiO_2-I-9 and Au/TiO_2-II-9 samples according to both TEM and EP analysis (not shown). Both samples had a smaller mean pore size as compared to that of the titania support (3.5 ± 0.2 nm) due to a partial pore blockage by the Au nanoparticles.

3.3. Catalytic tests in the hydrogenation of citral

Citral hydrogenation has been chosen as a test reaction as this is a multi-step reaction and the presence of internal diffusion limitations substantially decreases the selectivity towards the semihydrogenated products (unsaturated alcohols, nerol and geraniol (UCOL) and/or saturated aldehyde citronellal (CAL), Scheme 1). Citral conversion linearly increased with time from the beginning of the reaction, demonstrating the zero reaction order for citral (Fig. 11). A citral conversion of 81.2% was achieved after a reaction

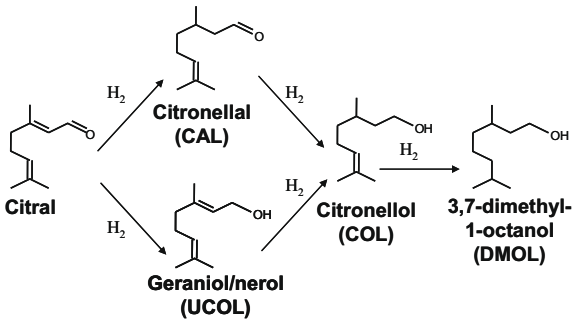

Scheme 1. Main products in citral hydrogenation.

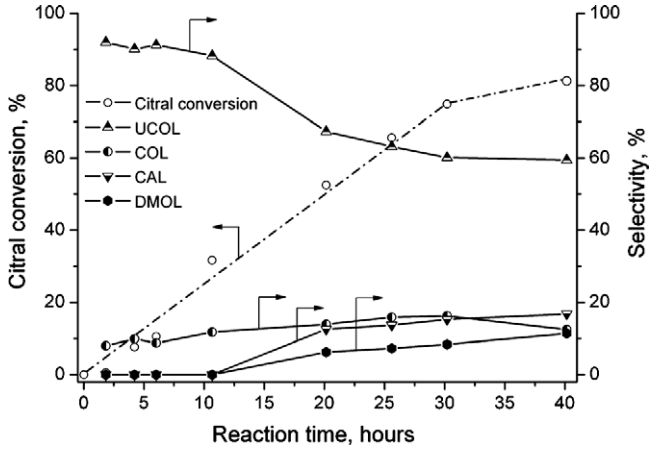

Fig. 11. Citral conversion and products selectivity on Au/TiO_2-I-9 as a function of the reaction time. Reaction conditions: temperature 343 K, 12 bar H_2, 0.01 M citral solution in 2-propanol, stirring speed 1500 rpm, catalyst mass 0.6 mg.

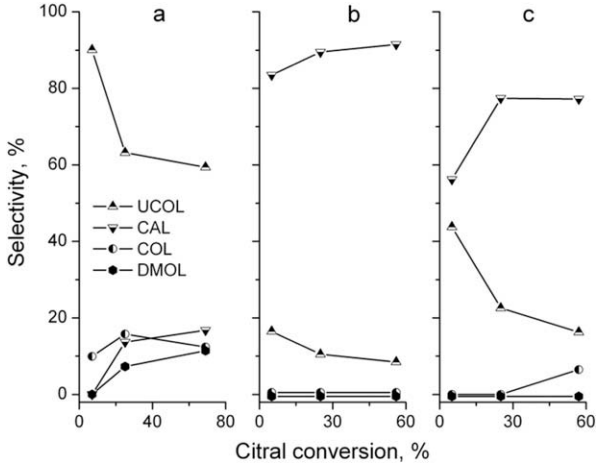

Fig. 12. Selectivity as a function of the citral conversion over (a) Au/TiO_2-I-9; (b) Au/TiO_2-II-9; (c) Au/TiO_2-V-9. Reaction conditions are the same as those in Fig. 11. The weights of the catalytic coatings are 0.6, 1.3 and 2.0 mg for (a), (b) and (c), respectively.

Table 4
Characteristics of the Au/TiO_2-*i*-9 thin films.

Parameter	Value
Apparent density (kg m^{-3})	400
Metal dispersion (–)	0.2
Au loading (wt.%)	1.0
Volumetric reaction rate ($m_L^3\ m_{cat}^{-3}\ s^{-1}$)	1.4
Film porosity (–)	0.3

time of 40 hours over Au/TiO_2-I-9. In the beginning of hydrogenation, UCOL was the main product with a selectivity as high as 90% while the hydrogenation of the C=C double bond was completely suppressed. Further hydrogenation of unsaturated alcohols resulted in the increase of selectivity to citronellol (COL) up to 14.5%. At a citral conversion of 70%, citronellal and 3,7-dimethyl-octanol (DMOL) were produced with a selectivity of 15.3% and 8.4%, respectively (Fig. 12a).

The thicker films (Au/TiO_2-II-9 and Au/TiO_2-V-9) showed a lower selectivity to the unsaturated alcohols as compared with Au/TiO_2-I-9 (Fig. 12b and c). Citronellal was the main product on the multilayered films with a substantial amount of citronellol at the end of the hydrogenation runs. Formation of the fully saturated product (3,7-dimethyl-1-octanol) was not observed.

The maximum coating thickness (h) to avoid internal diffusion limitations can be estimated for a zero-order reaction as $h = c/(k_v/D_e)^{0.5}$, where k_v is the volumetric reaction rate (see Table 4) and D_e is the effective diffusivity in the mesoporous network and c is a constant which depends on the reaction order and the catalyst geometry [40].

The maximum coating thickness for a single plate was found to be 5 μm in the beginning of the reaction run, when the zero-order in citral was observed. This is in line with the observed selectivity patterns. The selectivity towards the fully hydrogenated product was rather low over Au/TiO_2-V-9 even at high citral conversions.

It should be mentioned that at higher citral conversions, the reaction order with respect to citral gradually increased towards 1 and the maximum thickness to avoid internal diffusion limitations decreased to 0.7 μm. Therefore, the effective reaction rate over Au/TiO_2-V-9 was lower than the intrinsic rate observed over Au/TiO_2-II-9. From the effective reaction rate it is possible to estimate the effective diffusion coefficient of citral in catalytic films (D_{eff}) which is related to the molecular diffusion coefficient of citral (D_m) by Eq. (2).

$$D_{eff} = \frac{\varepsilon\sigma}{\tau} D_m \tag{2}$$

For the case considered in this study, $D_{eff} = 9 \times 10^{-12}$ m^2/s, $D_m = 2 \times 10^{-10}$ m^2/s, the tortuosity factor (τ) is assumed to be 1, and the mean porosity (ε) is equal to 0.3 giving the constriction factor (σ) of 0.15. Such a low value for the constriction factor indicates that the Au nanoparticles substantially reduce effective cross-sectional area available for reactant diffusion.

The initial intrinsic reaction rate in terms of TOF was ca. 1.4, 0.7 and 0.9 s^{-1} over Au/TiO_2-I-9, Au/TiO_2-II-9 and Au/TiO_2-V-9, respectively. In the absence of internal diffusion limitations, such differences can be related to different electronic states of the Au nanoparticles in thin (Au/TiO_2-I-9) and thick (Au/TiO_2-II-9, Au/TiO_2-V-9) films. In Au/TiO_2-I-9, the titanium substrate has a much larger influence on the electronic state of the titania film, which might substantially change the electronic properties of the embedded gold nanoparticles. There was also a dramatic change in the selectivity pattern between thin and thick catalytic films (Fig. 12): unsaturated alcohols were the main products over Au/TiO_2-I-9 while the yield of saturated aldehyde was much higher over the thicker films. A similar enhancement of the reaction rate as compared to that over the bulk material was observed in the water–gas shift reaction when a thin film of molybdenum carbide catalyst with a thickness of 50 nm was deposited on a molybdenum substrate [41]. However, this effect mostly disappeared in a thicker film, when the thickness of the Mo_2C layer was increased up to several microns.

It should be mentioned that the transport mechanisms within mesopores can be different. These include Knudsen diffusion, molecular diffusion in disordered domains and diffusion in the capillary-condensed phase [42]. In a three-phase reactor, the catalyst is usually contacted by a single fluid phase. However the pores can be emptied by vaporization, the necessary energy for which is supplied in part by the reaction heat. Reaction in the gas-filled pores can dominate even if the coating is mostly filled with liquid. This might explain observed small deviations in the initial reaction rate between Au/TiO_2-II-9 and Au/TiO_2-V-9.

TEM images of Au/TiO_2-II-9 (both fresh and after reaction) are shown in Fig. 13a and b. Disordered mesoporous domains can be seen after the reaction, however the Au nanoparticles maintained their initial size of 4.5 nm.

From the TEM images it is difficult to assess the location of nanoparticles, however, the following hypothesis may be drawn. Lower diffusivity of citral as compared to that expected in completely open mesopores and smaller pore size in the catalytic films from the EP analysis demonstrate that nanoparticles are partially embedded into the amorphous titania wall. The unit cell, which comprises one pore and the wall between two adjacent pores, is equal to 8.1 nm (Fig. 7). Therefore, the pore wall thickness is estimated to be 4.5 nm. The nanoparticles with a size smaller than the pore wall thickness can be in principle fully embedded into the wall. Even in that case, nanoparticles can be accessible for the reactants via micropores. A significant and unique feature of polymer templated mesoporous titania films is the presence of complimentary microporosity in the amorphous titania walls. These complementary pores interconnect adjacent mesopores which allows reactants to diffuse to the nanoparticles embedded into the wall. However in this study, the mean nanoparticle size is about the same as the pore wall thickness.

On the other hand, if the nanoparticles are located outside the mesoporous network, then the effective diffusivity of citral should be much higher. From the TEM, EP and kinetic measurement analysis, it can be concluded that nanoparticles are partially embedded into the titania wall and to some extent are protruded towards the adjacent mesopore but not fully blocking them.

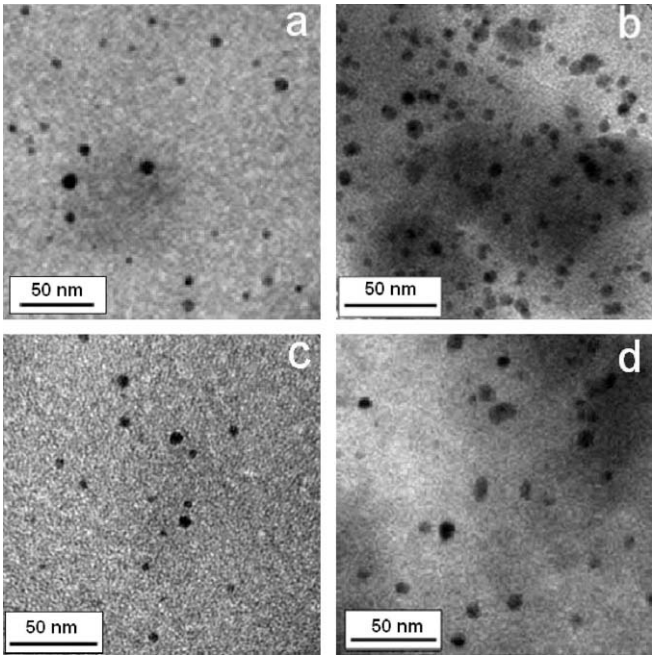

Fig. 13. TEM images of the mesoporous Au/TiO_2 films: (a) fresh Au/TiO_2-II-9, (b) Au/TiO_2-II-9 after reaction, (c) fresh Au/TiO_2-V-9, and (d) Au/TiO_2-V-9 after reaction.

The mean Au particle size in Au/TiO_2-V-9 after the reaction (Fig. 13d) was larger (7.0 nm) as compared to that in the fresh film (Fig. 13c). This film has larger disordered areas which can result in two diffusional pathways characterized by different diffusivities, namely those in the inner pore space and those between the ordered domains (Fig. 13c and d). A slightly larger gold nanopaticle size might be responsible for a higher initial TOF over Au/TiO_2-V-9 as compared to that expected if the intrinsic activity of Au would remain constant.

No deactivation was observed over Au/TiO_2-I-9 and Au/TiO_2-II-9 during the whole reaction period, while the TOF decreased from 0.9 to 0.26 s^{-1} over Au/TiO_2-V-9 within the first hour of reaction. It appears that the agglomeration of Au nanoparticles, which are not fully embedded into mesoporous domain, led to irreversible deactivation [43]. The deactivation could also be due to a partial collapse of the mesoporous network in Au/TiO_2-V-9. As a result, larger mesopores are formed and the Au nanoparticles can be physically blocked. However, a detailed study on the origin of deactivation of Au/TiO_2-V-9 was beyond the scope of this paper and will be reported elsewhere.

The new method of making mesoporous catalytic thin films allows to control the chemical nature of the film, its porous structure, thickness and loading with an active metal, as well as provides the "freedom of choice" of the catalytic species, which can further be fine tuned to fit specific applications. In addition to the Au nanoparticles considered in this study for the hydrogenation of citral, Pd nanoparticles can also be embedded into mesoporous titania films for the selective hydrogenation of phenylacetylene to styrene [44], while PdZn bimetallic nanoparticles can be employed in semihydrogenation of terminal acetylene alcohols to ethylene alcohols [45]. Successful implementation of this method will further depend on the capability of scaling the synthetic protocol from a substrate of a few square centimetres to that of a few meters while maintaining film uniformity.

4. Conclusions

Control of the thickness of mesoporous titania films deposited on a variety of substrates was achieved by multiple spin-coating. The thickness gain with each deposition cycle consistently decreased from ca. 300 nm per cycle in the first cycle to 200 nm in the last cycle. Gold nanoparticles with an average size of 4.5 nm were embedded in mesoporous titania films by the condensation of metal oxide species via self-assembly in the presence of a known amount of gold colloids. The complete surfactant removal leading to thermally stable mesoporous films was achieved at 573 K under a residual pressure of 10 mbar within 4 h. Under these conditions the Ti^{4+} sites were reduced to Ti^{3+} which might be responsible for a high selectivity to the unsaturated alcohols in the hydrogenation of citral over Au-containing supported catalysts.

Acknowledgments

The authors thank Dr. M. Creatore from Eindhoven University of Technology, Department of Applied Physics for providing an ellipsometer, Mr. V. Kuznetsov and Dr. E.A. Paukshtis from Boreskov Institute of Catalysis (Novosibirsk, Russia) for help in the FTIR study, Dr. P.A. Albouy from Laboratoire de Physique des Solides, Université Paris-Sud, France for 2D SAXS measurements, Mr. A. Ishchenko from Boreskov Institute of Catalysis and Mr. S. Çelebi from Eindhoven University of Technology, Department of Chemical Engineering and Chemistry for the TEM-measurements, and Mr. C. Buijs from Eindhoven University of Technology, Department of Chemical Engineering and Chemistry for SEM-measurements. The financial support by the Netherlands Organization for

Scientific Research (NWO) and the Russian Foundation for Basic Research (RFBR) in frame of NWO-RFBR Project 047.017.028, is gratefully acknowledged.

References

[1] V. Hessel, S. Hardt, H. Löwe, A. Müller, G. Kolb, Chemical Micro Process Engineering, Wiley, Belgium, 2005.
[2] V. Hessel, S. Hardt, H. Löwe, Chemical Micro Process Engineering: Fundamentals, Modelling and Reactions, Wiley, Belgium, 2004.
[3] E.V. Rebrov, G.B.F. Seijger, H.P.A. Calis, M.H.J.M. de Croon, C.M. van den Bleek, J.C. Schouten, Appl. Catal. A 206 (2001) 125.
[4] M.J.M. Mies, J.L.P. van den Bosch, E.V. Rebrov, J.C. Jansen, M.H.J.M. de Croon, J.C. Schouten, Catal. Today 110 (2005) 38.
[5] M.J.M. Mies, E.V. Rebrov, J.C. Jansen, M.H.J.M. de Croon, J.C. Schouten, Microporous Mesoporous Mater. 106 (2007) 95.
[6] M.J.M. Mies, E.V. Rebrov, J.C. Jansen, M.H.J.M. de Croon, J.C. Schouten, J. Catal. 247 (2007) 328.
[7] O. Muraza, E.V. Rebrov, J. Chen, M. Putkonen, L. Niinistö, M.H.J.M. de Croon, J.C. Schouten, Chem. Eng. J. 135S (2008) S117.
[8] E.V. Rebrov, M.H.J.M. de Croon, J.C. Schouten, Catal. Today 69 (2001) 183.
[9] I.Z. Ismagilov, R.P. Ekatpure, L.T. Tsykoza, E.V. Matus, E.V. Rebrov, M.H.J.M. de Croon, M.A. Kerzhentsev, J.C. Schouten, Catal. Today 105 (2005) 516.
[10] D. Grosso, F. Cagnol, G.J. de. A.A. Soler-Illia, E.L. Crepaldi, H. Amenitsch, A. Brunet-Bruneau, A. Bourgeois, C. Sanchez, Adv. Funct. Mater. 14 (2004) 309.
[11] L. Malfatti, P. Falcaro, H. Amenitsch, S. Caramori, R. Argazzi, C.A. Bignozzi, S. Enzo, M. Maggini, P. Innocenzi, Microporous Mesoporous Mater. 88 (2006) 304.
[12] O. Muraza, E.V. Rebrov, T. Khimyak, B.F.G. Johnson, P.J. Kooyman, U. Lafont, P.A. Albouy, M.H.J.M. de Croon, J.C. Schouten, Stud. Surf. Sci. Catal. 162 (2006) 167.
[13] T.S. Glazneva, E.V. Rebrov, J.C. Schouten, E.A. Paukshtis, Z.R. Ismagilov, Thin Solid Films 515 (2007) 6391.
[14] O. Muraza, E.V. Rebrov, T. Khimyak, B.F.G. Johnson, P.J. Kooyman, U. Lafont, M.H.J.M. de Croon, J.C. Schouten, Chem. Eng. J. 135 (2008) S99.
[15] E.L. Crepaldi, G.J. de A.A. Soler-Illia, D. Grosso, F. Cagnol, F. Ribot, C. Sanchez, J. Am. Chem. Soc. 125 (2003) 9770.
[16] Y. Zhang, A.H. Yuwono, J. Li, J. Wang, Microporous Mesoporous Mater. 110 (2008) 242.
[17] D.M. Antonelli, Microporous Mesoporous Mater. 30 (1999) 315.
[18] U.-H. Lee, H. Lee, S. Wen, S. Mho, Y.-U. Kwon, Microporous Mesoporous Mater. 88 (2006) 48.
[19] D. Grosso, F. Babonneau, C. Sanchez, G.J. de A.A. Soler-Illia, E.L. Crepaldi, J. Sol–Gel Sci. Technol. 26 (2003) 561.
[20] J. Sabataityteÿ, I. Oja, F. Lenzmann, O. Volobujeva, M. Krunks, Preliminary communication, C.R. Chimie 9 (2006) 708.
[21] Y.K. Hwang, K.-C. Lee, Y.-U. Kwon, The Royal Society of Chemistry, Chem. Commun. (2001) 1738.
[22] M. Wark, J. Tschirch, O. Bartels, D. Bahnemann, J. Rathouskyr', Microporous Mesoporous Mater. 84 (2005) 247.
[23] M.C. Fuertes, M. Marchena, M.C. Marchi, A. Wolosiuk, G.J.A.A. Soler-Illia, Small 5 (2009) 272.
[24] E.V. Rebrov, A. Berenguer-Murcia, B.F.G. Johnson, J.C. Schouten, Catal. Today 138 (2008) 210.
[25] P. Lu, T. Teranishi, K. Asakura, M. Miyake, N. Toshima, J. Phys. Chem. B 103 (1999) 9673.
[26] S. Domínguez-Domínguez, A. Berenguer-Murcia, D. Cazorla-Amorós, A. Linares-Solano, J. Catal. 243 (2006) 74.
[27] E.A. Paukshtis, IR-spectroscopy in heterogeneous acid–basic catalysis, Science, Russia, Novosibirsk, 1992, p. 47.
[28] L.N. Protasova, E.V. Rebrov, Z.R. Ismagilov, J.C. Schouten, Microporous Mesoporous Mater. 123 (2009) 243.
[29] M. Boudart, Kinetics of Heterogeneous Catalytic Reactions, Princeton University Press, Princeton, NJ, 1984. p. 26.
[30] M. Klotz, P.-A. Albouy, A. Ayral, C. Menager, D. Grosso, A. van der Lee, V. Cabuil, F. Babonneau, C. Guizard, Chem. Mater. 12 (2000) 1721.
[31] IUPAC Recommendations, Pure Appl. Chem. 66 (1994) 1739.
[32] G. Busca, H. Saussey, O. Saur, J.C. Lavalley, V. Lorenzelli, Appl. Catal. 14 (1985) 245.
[33] K. Kim, Bull. Korean Chem. Soc. 11 (1990) 396.
[34] T. Ekou, A. Vicente, G. Lafaye, C. Especel, P. Marecot, Appl. Catal. A 314 (2006) 73.
[35] Y. Li, B. Xu, Y. Fan, N. Feng, A. Qiu, J.M.J. He, H. Yang, Y. Chen, J. Mol. Catal. A 216 (2004) 107.
[36] P. Mäki-Arvela, J. Hajek, T. Salmi, D.Yu. Murzin, Appl. Catal. A 292 (2005) 1.
[37] L. Bonneviot, G. Haller, J. Catal. 113 (1988) 96.
[38] M.M. Viana, T.D.S. Mohallem, G.L.T. Nascimento, N.D.S. Mohallem, Braz. J. Phys. 36 (2006) 1081.
[39] J.C. Yu, J. Yu, W. Ho, J. Zhao, J. Photochem. Photobiol. A 148 (2002) 331–339.
[40] C.N. Satterfield, Mass Transfer in Heterogeneous Catalysis, MIT Press, England, Cambridge, 1970.
[41] E.V. Rebrov, S.A. Kuznetsov, M.H.J.M. de Croon, J.C. Schouten, Catal. Today 125 (2007) 88.
[42] R. Valiullin, J. Karger, R. Glaser, Phys. Chem. Chem. Phys. 11 (2009) 2833.
[43] P. Konova, A. Naydenov, C. Venkov, D. Mehandjiev, D. Andreeva, T. Tabakova, J. Mol. Catal. A 213 (2004) 235.
[44] E.V. Rebrov, A. Berenguer-Murcia, H.E. Skelton, B.F.G. Johnson, A.E.H. Wheatley, J.C. Schouten, Lab Chip 9 (2009) 503.
[45] E.V. Rebrov, E.A. Klinger, A. Berenguer-Murcia, E. Sulman, J.C. Schouten, Org. Process. Res. Dev. (2009), doi:10.1021/op900085b.
[46] A. Dey, S. Karan, S.K. De, Solid State Ionics 178 (2008) 1963.
[47] J.K. Walters, R.J. Newport, J. Phys.: Condens. Matter 7 (1995) 1755.
[48] P.J. Kruegearn, D.J. Jan, Can. J. Chem. 48 (1970) 3236.
[49] J. Heidberg, E. Kampshoff, R. Kiihnemuth, O. Schönekiis, Surf. Sci. 269/270 (1992) 120.
[50] A. Grodzicki, P. Piszczek, J. Mol. Struct. 443 (1998) 141.
[51] Y. Kim, M. Yoon, J. Mol. Catal. A 168 (2001) 257.